Finite Elements in Analysis and Design ∎ (∎∎∎∎) ∎∎∎–∎∎∎

Contents lists available at ScienceDirect

Finite Elements in Analysis and Design

journal homepage: www.elsevier.com/locate/finel

Full Length Article

Modelling the failure of reinforced concrete with nonlocal and crack band approaches using the damage-plasticity model CDPM2

Dimitrios Xenos [a,b], Peter Grassl [b,*]

[a] Special Services Division, Mott MacDonald Ltd, UK
[b] School of Engineering, University of Glasgow, Glasgow, UK

ARTICLE INFO

Article history:
Received 13 August 2015
Received in revised form
10 April 2016
Accepted 10 April 2016

Keywords:
Nonlocal
Damage
Concrete
Steel reinforcement
Fracture

ABSTRACT

A nonlocal extension of the damage-plasticity model CDPM2 is proposed. The performance of this extension is evaluated in comparison with a crack band version of the same model for describing the failure of reinforced concrete. In particular, the influence of mesh size on the structural response in the form of load–displacement curves and strain distributions is studied for a reinforced concrete beam subjected to four point bending. The nonlocal model provides mesh independent load–displacement curves and strain profiles, whereas the peak loads and strain profiles obtained with the crack band model depend on the element size.

1. Introduction

The failure process of reinforced concrete is complex, since its constituents in the form of concrete and reinforcement and their interaction exhibit strongly nonlinear mechanical responses. For instance, the response of plain concrete depends strongly on the type of loading applied. In tension, concrete exhibits a quasi-brittle softening response (decreasing stress with increasing displacements), whereas for confined compression hardening (increasing stress with increasing displacements) is observed. It is important to consider these nonlinearities for the modelling of shear and compressive failure processes in reinforced concrete structures.

The finite element method has the potential to predict the nonlinear response of reinforced concrete structures based on the spatial arrangement and properties of its constituents. However, constitutive models for concrete, reinforcement and its interaction are required, which describe the material behaviour mesh objectively considering all important features observed in experiments. For concrete, this is not a straightforward task due to the complexity of the material response. The model should be advanced enough to capture the different responses in tension, and low and high confined compression, be easy to calibrate, and be formulated in a way that the results are insensitive to the size and orientation of finite elements. One well-known group of models, which are often employed to ensure a mesh independent description of the failure of concrete, are integral type nonlocal approaches [28]. In these models, the stress at a point is evaluated as a spatial weighted average of history variables in the vicinity of this point. These models produce fracture patterns independently of the mesh for both localised and distributed cracking, and are insensitive to the finite element mesh alignment [2]. Therefore, they are more versatile than cohesive crack and crack band models [5], which have been shown to be sensitive to the mesh alignment [19] and, for distributed cracking, on the mesh size [14]. Many different nonlocal models have been proposed in the literature. For instance, a number of different averaging functions based on distances to boundaries [8,20,4] and stress states [1,11,15] have been proposed. However, most of these models have been evaluated by analysing structures made of plain concrete. Less research has been performed to investigate the performance of nonlocal models to simulate reinforced concrete structures [26,22], despite virtually all concrete structures being reinforced. Furthermore, many previous studies are limited to very simplified constitutive models, which are not capable to describe the complex response of concrete structures subjected to multiaxial stress states. Therefore, there is more room for research to evaluate nonlocal extensions of advanced constitutive models for the analysis of reinforced concrete structures to bridge the gap between theoretical constitutive modelling and structural engineering application.

The aim of the present study is to investigate the performance of nonlocal models for analysing the response of reinforced

* Corresponding author. Tel.: +44 141 330 5208.
E-mail address: peter.grassl@glasgow.ac.uk (P. Grassl).

http://dx.doi.org/10.1016/j.finel.2016.04.002

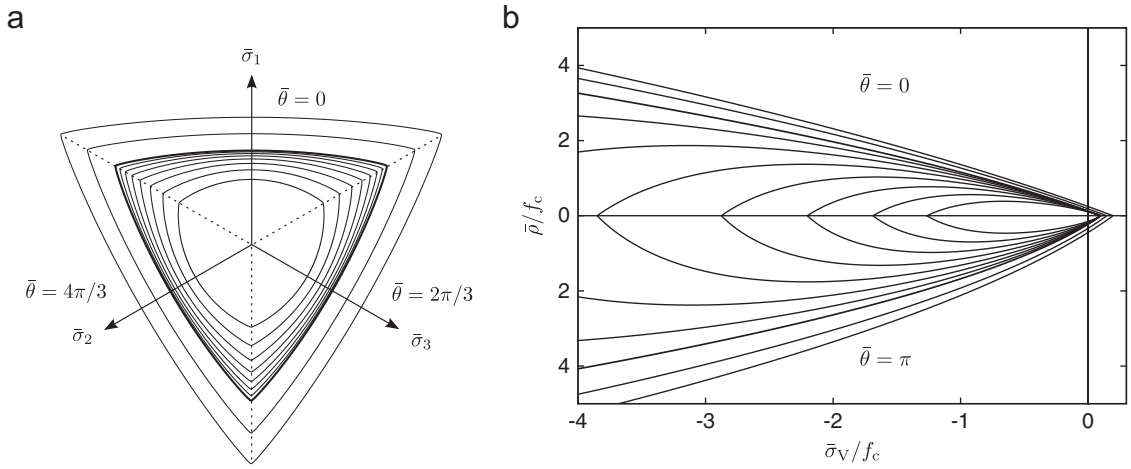

Fig. 1. Yield function: (a) evolution of the deviatoric section of the yield surface during hardening for a constant volumetric stress of $\bar{\sigma}_v = -f_c/3$. (b) Evolution of the meridional section of the yield surface during hardening in the pre-peak and post-peak regime. The peak is indicated by a thicker line.

concrete structures, and to compare these results to those obtained with crack band approaches. In particular, the influence of the mesh size on global load–displacement curves and local crack patterns will be investigated for these two approaches. Special emphasis is placed on using a constitutive model capable of capturing the important features of the nonlinear mechanical response of concrete.

The constitutive model used for the the nonlocal and crack band approach is the damage-plasticity model CDPM2, which was originally proposed in Grassl et al. [16] and is an extension of the damage-plastic model presented in Grassl and Jirásek [13]. This model is based on a combination of effective stress based plasticity and isotropic damage. The plasticity part uses a yield surface based on a strength envelope proposed in Menétrey and Willam [24], which incorporates concrete specific features such as curved meridians and deviatoric sections varying from triangular shapes in tension to almost circular shapes in confined compression. Together with a pressure sensitive hardening law, the pressure dependence of strength and peak strain are described. The damage part uses damage variables for tensile and compressive dominant stress states following the approaches proposed in Mazars [23], Ortiz [25], and Fichant et al. [10]. It describes the reduction of stiffness in tension and low confined compression, as well as stiffness recovery for the transition from tension to compression. The proposed nonlocal extension of the model in the present study has not been presented before.

Firstly, the performances of the nonlocal and the crack-band models are investigated for uniaxial tension of an unreinforced specimen and a three point bending test to demonstrate the techniques used to describe fracture in plain concrete mesh independently. Then, the models are applied to the analysis of a reinforced concrete beam [21], which was selected, because it exhibits both localised and distributed cracking. This test involves failure modes, which, both on the material and structural level, are challenging to model. Therefore, this is a suitable test to evaluate the capabilities of the present modelling approaches to describe the experimental results mesh independently. Furthermore, the influence of the interaction radius of nonlocal models on the prediction of crack patterns is investigated.

2. Constitutive model

The constitutive model used for the analysis of reinforced concrete is based on the damage-plasticity concrete model CDPM2 [16], which is an extension of CDPM [13]. In the present section, a brief overview of the main formulation of this constitutive model and its nonlocal and crack band extensions are presented. The nominal stress is evaluated as

$$\boldsymbol{\sigma} = (1-\omega_t)\overline{\boldsymbol{\sigma}}_t + (1-\omega_c)\overline{\boldsymbol{\sigma}}_c \tag{1}$$

where ω_t and ω_c are two scalar damage parameters, ranging from 0 (undamaged) to 1 (fully damaged). The stress components $\overline{\boldsymbol{\sigma}}_t$ and $\overline{\boldsymbol{\sigma}}_c$ are the tensile and compressive part, respectively, of the effective stress

$$\overline{\boldsymbol{\sigma}} = \boldsymbol{D}_e(\boldsymbol{\varepsilon} - \boldsymbol{\varepsilon}_p) \tag{2}$$

where $\boldsymbol{D}_e$ is the elastic stiffness, $\boldsymbol{\varepsilon}$ is the strain and $\boldsymbol{\varepsilon}_p$ is the plastic strain. The split of the effective stress into tensile and compressive parts is performed in the principal stress space. Firstly, the principal effective stress $\overline{\boldsymbol{\sigma}}_P$ is split into $\overline{\boldsymbol{\sigma}}_{Pt} = \langle \overline{\boldsymbol{\sigma}}_P \rangle_+$ and $\overline{\boldsymbol{\sigma}}_{Pc} = \langle \overline{\boldsymbol{\sigma}}_P \rangle_-$, which are the positive and negative parts, respectively. Then, $\overline{\boldsymbol{\sigma}}_{Pt}$ and $\overline{\boldsymbol{\sigma}}_{Pc}$ are expressed in the original coordinate system to form $\overline{\boldsymbol{\sigma}}_t$ and $\overline{\boldsymbol{\sigma}}_c$.

The plastic strains in (2) are evaluated by the plasticity part of the model, which consists of the yield function, hardening functions, flow rule and loading and unloading conditions. The yield function f_p is formulated using the Haigh–Westergaard coordinates, which are the volumetric effective stress $\bar{\sigma}_v$, the length of the deviatoric effective stress $\bar{\rho}$ and the Lode angle $\bar{\theta}$. The meridians of the yield surface ($f_p = 0$) are parabolic and the deviatoric sections vary from being triangular at low confinement to almost circular in high confinement. The evolution of the yield surface, shown in Fig. 1, is described by two hardening functions $q_{h1}(\kappa_p)$ and $q_{h2}(\kappa_p)$, which are controlled by the hardening variable κ_p defined in rate form as

$$\dot{\kappa}_p = \frac{\| \dot{\boldsymbol{\varepsilon}}_p \|}{x_h(\bar{\sigma}_v)} \tag{3}$$

The hardening functions are shown in Fig. 2(a). At $q_{h1} = q_{h2} = 1$, the peak has been reached at which stage the yield surface coincides with the failure surface proposed in Menétrey and Willam [24], which is shown in Fig. 1 by a thicker line. In (3), the variable x_h is a hardening ductility measure, which is a function of the effective volumetric stress. It is used to provide a greater strain capacity in confined compression than in uniaxial compression and tension.

The flow rule provides the direction of the plastic flow

$$\dot{\boldsymbol{\varepsilon}}_p = \dot{\lambda}\frac{\partial g_p}{\partial \overline{\boldsymbol{\sigma}}} \tag{4}$$

Here, function g_p is the plastic potential function, and $\dot{\lambda}$ is the rate of the plastic multiplier. In CDPM2, the flow rule is non-associated,

Please cite this article as: D. Xenos, P. Grassl, Modelling the failure of reinforced concrete with nonlocal and crack band approaches using the damage-plasticity model CDPM2, Finite Elem. Anal. Des. (2016), http://dx.doi.org/10.1016/j.finel.2016.04.002

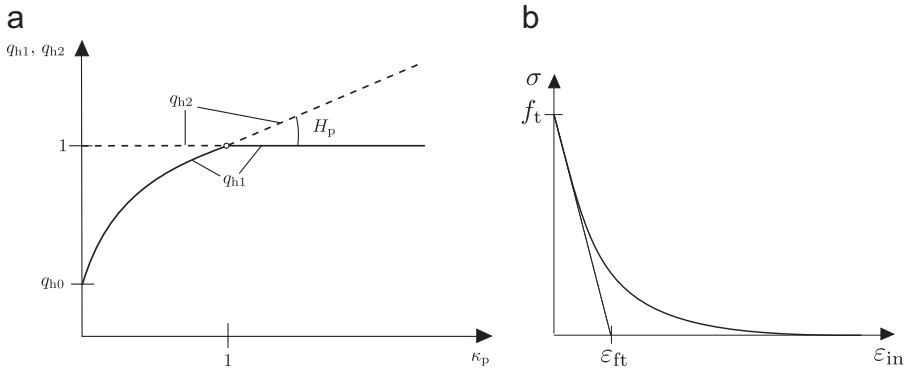

Fig. 2. (a) Hardening laws of the plasticity part. (b) Exponential softening law for the damage part.

i.e. the yield function f_p and the plastic potential g_p do not coincide, which results in a better description of the volumetric expansion during confined compressive stress states [12]. Finally, the loading–unloading conditions

$$f_p \le 0, \dot{\lambda} \ge 0, \dot{\lambda} f_p = 0 \tag{5}$$

complete the description of the plasticity part. A detailed description of the individual components outlined above are described in Grassl et al. [16] and Grassl and Jirásek [13].

In the damage part of the model, the evolution of ω_t and ω_c is controlled, among others, by the tensile and compressive equivalent strains, $\tilde{\varepsilon}_t$ and $\tilde{\varepsilon}_c$, respectively. The tensile equivalent strain $\tilde{\varepsilon}_t$ is a function of the effective stress $\overline{\boldsymbol{\sigma}}$. For the special case of 1D tension, it simplifies to $\tilde{\varepsilon}_t = \overline{\sigma}/E$, where E is Young's modulus. The compressive equivalent strain $\tilde{\varepsilon}_c$ is defined in rate form as

$$\dot{\tilde{\varepsilon}}_c = \alpha_c \dot{\tilde{\varepsilon}}_t \tag{6}$$

The variable α_c is used to distinguish between tensile and compressive stress states. It ranges from 0 for pure tensile to 1 for pure compressive stress states. This allows for the modelling of the apparent stiffness recovery during the transition from tension to compression. The history variables, which enter the damage functions, form two groups of three variables each, which are related to the tensile and the compressive part, respectively. They are

$$\kappa_{dt} = \max_{\tau \le t} \tilde{\varepsilon}_t, \quad \dot{\kappa}_{dt1} = \frac{\| \dot{\boldsymbol{\varepsilon}}_p \|}{\chi_s(\overline{\sigma}_v, \overline{\rho})}, \quad \dot{\kappa}_{dt2} = \frac{\dot{\kappa}_{dt}}{\chi_s(\overline{\sigma}_v, \overline{\rho})}$$
$$\kappa_{dc} = \max_{\tau \le t} \tilde{\varepsilon}_c, \quad \dot{\kappa}_{dc1} = \frac{\alpha_c \beta_c \| \dot{\boldsymbol{\varepsilon}}_p \|}{\chi_s(\overline{\sigma}_v, \overline{\rho})}, \quad \dot{\kappa}_{dc2} = \frac{\dot{\kappa}_{dc}}{\chi_s(\overline{\sigma}_v, \overline{\rho})} \tag{7}$$

Here, the ductility measure χ_s is a function of $\overline{\sigma}_v$ and $\overline{\rho}$, which takes into account the influence of multiaxial stress states on the damage evolution. Exponential damage laws are used in which the initial slope of the softening curve is controlled by the strain threshold parameters, ε_{ft} and ε_{fc} for tension and compression, respectively, which is shown for the case of tension in Fig. 2(b). In this figure, ε_{in} is the inelastic strain in tension composed of both reversible and irreversible inelastic strain components expressed as

$$\varepsilon_t^{in} = \kappa_{dt1} + \omega \kappa_{dt2} \tag{8}$$

In compression the inelastic strain and the history and damage variables are replaced by their compressive counterparts.

CDPM2 requires a large number of input parameters, for the elastic, plastic and damage parts. However, in the present paper, only a few parameters are calibrated, namely the tensile strength f_t, the compressive strength f_c and the tensile damage threshold ε_{ft}, which is related to the fracture energy G_F. Furthermore, the strain threshold ε_{fc} and the parameter A_s in the damage ductility measure were chosen as 3×10^{-5} and 15, respectively. The remaining parameters were set to their default values provided in Grassl et al. [16], where it was shown that these values provide a good fit with a wide range of experimental results.

2.1. Nonlocal approach

The integral type nonlocal approach is applied to CDPM2 to provide mesh independent load–displacement curves and mesh independent localised fields of history variables. It is aimed to achieve this by evaluating the nonlocal history variables at a point $\boldsymbol{x}$ as the weighted average of the local history variables at all points $\boldsymbol{\xi}$ in the vicinity of $\boldsymbol{x}$ within the integration domain V. For a history variable f this is expressed as

$$\overline{f}(\boldsymbol{x}) = \int_V \alpha(\boldsymbol{x}, \boldsymbol{\xi}) f(\boldsymbol{\xi}) \, \mathrm{d}\boldsymbol{\xi} \tag{9}$$

According to the standard scaling approach originally proposed in Pijaudier-Cabot and Bažant [28], the weight function

$$\alpha(\boldsymbol{x}, \boldsymbol{\xi}) = \frac{\alpha_\infty(\boldsymbol{x}, \boldsymbol{\xi})}{\int_V \alpha_\infty(\boldsymbol{x}, \boldsymbol{\zeta}) \, \mathrm{d}\boldsymbol{\zeta}} \tag{10}$$

is constructed from a function α_∞ normalised by its integral over the integration domain V so that the averaging scheme does not modify a uniform field. In the present study, this weight function is

$$\alpha_\infty(\boldsymbol{x}, \boldsymbol{\xi}) = \exp\left(-\frac{\| \boldsymbol{x} - \boldsymbol{\xi} \|}{R} \right) \tag{11}$$

where R is the nonlocal interaction radius, which is a material parameter independent of the finite element size. The value of the interaction radius controls the width of nonlinear zones formed during failure. There is no direct link between experimentally measured fracture properties and the nonlocal interaction radius, because the width of the nonlinear zones depends also strongly on the selected weight function. However, R can be implicitly calibrated by comparison of the roughness of fracture surfaces and the dissipated energy fields as it was shown for example in [31]. In this study it was shown that the roughness depends also on the size of the inclusions which were modelled indirectly by an auto-correlated random field. Another calibration strategy has also been proposed in [6].

For CDPM2, the nonlocal averaging was applied to both the tensile and the compressive damage part. The variables $\tilde{\varepsilon}_t$, $\tilde{\varepsilon}_c$, κ_{dt1}, κ_{dc1}, κ_{2t} and κ_{2c} used in the damage laws were replaced by their nonlocal counterparts by averaging their rates using (9). Nonlocal averaging of all these variables is required to calculate the nonlocal inelastic strain ε_{in} given in its local form in (8). The nonlocal averaging is not applied to the plasticity part of the model. Therefore, the effective stress–strain part of the model remains local.

For calibrating the nonlocal version of CDPM2 for the two-dimensional analyses in Section 5, the softening strain threshold of the nonlocal model was determined by means of 1D uniaxial

Please cite this article as: D. Xenos, P. Grassl, Modelling the failure of reinforced concrete with nonlocal and crack band approaches using the damage-plasticity model CDPM2, Finite Elem. Anal. Des. (2016), http://dx.doi.org/10.1016/j.finel.2016.04.002

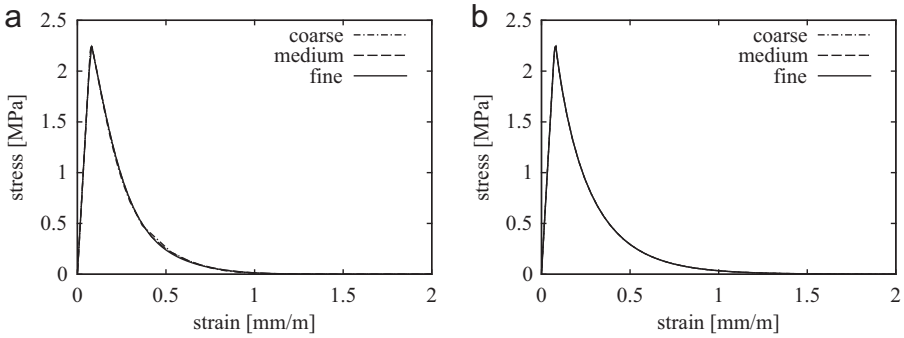

Fig. 3. Average stress–strain curves for the (a) nonlocal and (b) crack-band model for the 1D direct tension test for three different meshes.

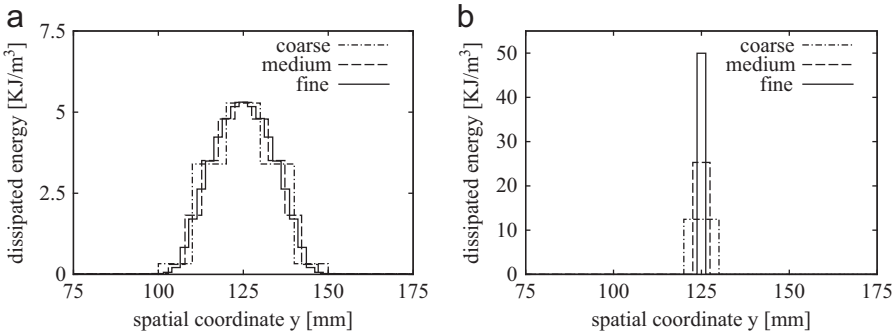

Fig. 4. Comparison of the dissipated energy density profiles for the analysis with the (a) nonlocal and (b) crack band model of the 1D direct tension test for three different meshes.

tensile analyses. Since in the 1D analyses the averaging in the lateral direction is not taken into account automatically, a modified weight function is used in the 1D analyses so that the results for one and two-dimensional analyses are the same, as long as they are not affected by boundaries. In Grassl et al. [15], it has been shown that this can be achieved by defining the averaging for the 1D case as

$$\overline{\epsilon}_{\mathrm{eq}}(z) = \int_{-\infty}^{\infty}\int_{-\infty}^{\infty} \alpha_{\infty}\left(\sqrt{(z-\xi)^2+s^2}\right)\epsilon_{\mathrm{eq}}(\xi)\, d\xi\, ds \tag{12}$$

where z is the coordinate along the 1D specimen. This approach was adopted in the present study. There is no closed form solution for the integral in (12) for the exponential weight function in (11), so that it is evaluated numerically.

2.2. Crack-band approach

The crack band approach for producing mesh independent load–displacement curves for fracture in plain concrete is based on the idea that the crack opening is transformed into inelastic strain by distributing it over an element length dependent zone [5]. This approach will only produce mesh independent load–displacement curves, if the inelastic strain profiles in the finite element analysis are mesh size dependent. This requirement is an important difference to the nonlocal model which is designed to produce both mesh size independent load–displacement curves and strain profiles. In CDPM2, the crack band approach is applied only to the tensile part of the damage algorithm by replacing the stress–inelastic strain law shown in Fig. 2(b) by a stress–inelastic displacement law of the form

$$\sigma = f_{\mathrm{t}} \exp\left(-\frac{\epsilon_{\mathrm{in}} h}{w_{\mathrm{ft}}}\right) \quad \text{if } (\epsilon_{\mathrm{in}} > 0) \tag{13}$$

Here, w_{ft} is a crack opening threshold used to control the slope of the softening curve and h is the width of the crack-band, which in the present study is equal to the maximum dimension of the element along the principal direction of the strain tensor corresponding to the maximum tensile principal strain at the onset of damage. For the compressive part, a stress–inelastic strain law was used to determine the compressive damage parameter, since it was reported in [14] for columns subjected to eccentric compression that inelastic strain profiles in compression do not exhibit a mesh dependence which would satisfy the assumptions of the crack-band approach. This approach of applying the crack-band approach only to the tensile part has already been successfully used in Grassl et al. [16].

3. Calibration

The constitutive model CDPM2 requires a large number of input parameters. However, the majority of these parameters have default values, which give acceptable results for standard concrete mixes. For a detailed description of the meaning of the input parameters and suggestions how to determine them, the reader is referred to Grassl and Jirásek [13] and Grassl et al. [16]. In the present calibration, the parameters $E = 30.5$ GPa, $\nu = 0.2$, $f_{\mathrm{c}} = 28.5$ MPa, $f_{\mathrm{t}} = 2.247$ MPa and $G_{\mathrm{F}} = 133$ N/m were determined using the CEB-FIB Model Code 2010 [9] for the compressive strength specified in [21].

For the crack band model, G_{F} can be directly related to the model parameter w_{ft}, as $w_{\mathrm{ft}} = G_{\mathrm{F}}/f_{\mathrm{t}} = 0.0594$ mm. For the nonlocal model, G_{F} is a function of parameters f_{t}, $\varepsilon_{\mathrm{ft}}$ and R without a closed form solution. Therefore, the parameter ε_{f} was determined inversely by analysing a 1D bar subjected to uniaxial tension used in the next Section 4 for a given f_{t} and R. For $R = 0.01$ m, the inverse calibration for $G_{\mathrm{F}} = 133$ N/m resulted in $\varepsilon_{\mathrm{ft}} = 0.00099$. For $R = 0.005$ m, $\varepsilon_{\mathrm{ft}} = 0.00179$.

Please cite this article as: D. Xenos, P. Grassl, Modelling the failure of reinforced concrete with nonlocal and crack band approaches using the damage-plasticity model CDPM2, Finite Elem. Anal. Des. (2016), http://dx.doi.org/10.1016/j.finel.2016.04.002

4. Uniaxial tensile and three point bending test of plain concrete

Two tests for fracture in plain concrete are performed to investigate how well the nonlocal and crack band model can describe the failure process in plain concrete mesh independently. The first analysis comprises a uniaxial tensile bar of 0.25 m length subjected to direct tension. In the middle of the bar, one element was slightly weakened to trigger localisation. The material parameters were chosen to be equal to those in Section 3 for $R=0.01$ m. A coarse, medium and fine mesh with 25, 51 and 101 elements, respectively, were used to discretise the tensile bar. In the nonlocal model, the modified averaging introduced in (12) was used, which allows for employing 1D elements for 2D nonlocal averaging, as described in Section 2.1. Both nonlocal and crack band approaches provide mesh independent average stress–strain curves shown in Fig. 3. The dissipated energy density profiles at the final loading step at an average strain of 2 mm/m are shown in Fig. 4 for the two models. The nonlocal approach provides mesh independent representations of the dissipated energy density profiles. It should be noted that this result is not always obtained for nonlocal damage-plasticity models, in which the averaging is only applied to the damage part. In Grassl and Jirásek [14], it was shown that if the local plasticity part exhibits perfect plasticity, the nonlocal damage-plasticity model results in mesh independent load–displacement curves but mesh dependent dissipated energy density profiles. The mesh independent energy density profiles are obtained in the present study because the plasticity part exhibits only hardening ($H_p > 0$). For this reason, the standard nonlocal formulation described in Section 2.1 provides mesh independent results and was applied in the analyses. In the analyses with the crack-band approach, the zone of dissipated energy is mesh dependent, as it is expected for plain concrete subjected to uniaxial tension.

In the second test of fracture in plain concrete, a beam subjected to three point bending is investigated. The geometry and the loading setup are shown in Fig. 5a. Three meshes with element lengths in the refined zone in the middle of the beam of 20, 10 and 5 mm were used for both the nonlocal and the crack band model (Fig. 5b).

The load–CMOD curves for the nonlocal and crack band approaches are shown in Fig. 6. Here, CMOD is defined as the relative horizontal displacement between points B and A shown in Fig. 5a.

Both models produce very similar load–CMOD curves for the different mesh sizes. The pre-peak response and the peak loads obtained with the nonlocal model for the three meshes are identical. Only for the coarse mesh, the post-peak part of the curves is steeper than the response obtained for the other meshes. Also for the crack band model the load–CMOD curves are not very sensitive to the mesh size. Only the peak differs significantly for the three meshes. The mesh dependencies observed for the two models can be understood by studying the contour plots of history variables. The contour plots of the principal strain are shown in Figs. 7 and 8 for the nonlocal and crack band model, respectively for a coarse, medium and fine mesh. The maximum principal strain contour plots for the nonlocal model demonstrate that for the coarse mesh only two elements are located in the localised strain region. As a result, there are not enough integration points located in the localised strain region to accurately calculate the nonlocal averages. Therefore, the energy dissipation in the post-peak is slightly less than for the other two meshes, which explains the difference in the load–CMOD curves in the post-peak regime. A small region of distributed strain is visible at the bottom of the beam, which is typical for analyses of unnotched structures. However, this distributed region does not introduce any mesh-size dependence. For the analyses with the crack band approach, the localised strain profiles are mesh-dependent which is a necessary requirement for the crack band approach to provide mesh independent load–CMOD curves. However, the zone of distributed damage at the bottom is not mesh dependent. Therefore, the peak loads of the crack band analyses are depend on the mesh size.

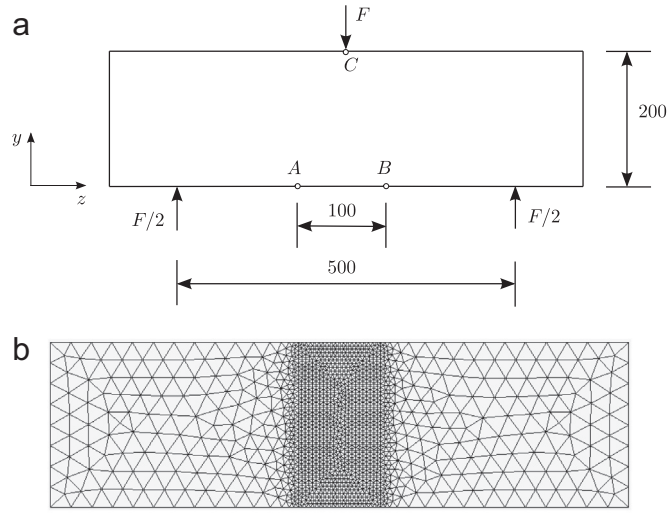

Fig. 5. Three point bending test of plain concrete: (a) geometry and loading setup of the analyses. (b) Fine mesh with an element length of approx. 5 mm.

5. Leonhardt and walter reinforced concrete beam

In this section, the results of the analysis of the reinforced concrete beam no. 5 from the series of experiments reported in Leonhardt and Walther [21] are described. In the experiment, the beam was subjected to four-point loading and exhibited shear

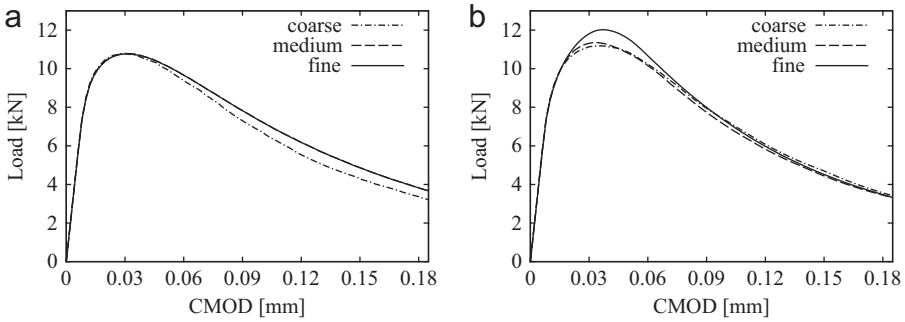

Fig. 6. Load–CMOD curves for the analyses with the (a) nonlocal and (b) crack band model of the three point bending test with different meshes.

Please cite this article as: D. Xenos, P. Grassl, Modelling the failure of reinforced concrete with nonlocal and crack band approaches using the damage-plasticity model CDPM2, Finite Elem. Anal. Des. (2016), http://dx.doi.org/10.1016/j.finel.2016.04.002

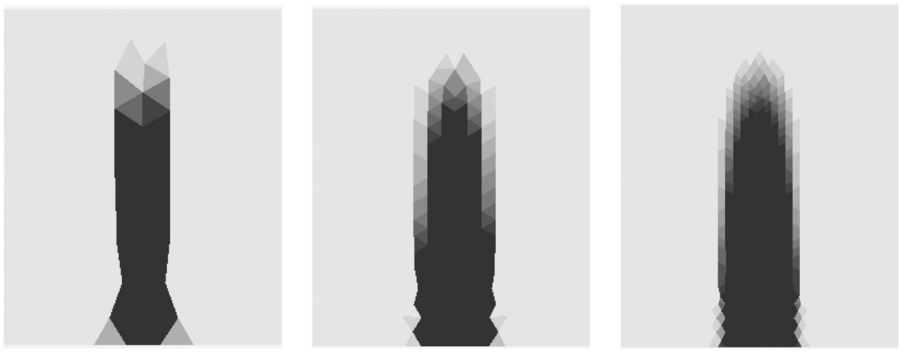

Fig. 7. Contour plots of the maximum principal strain ε_1 of the three point bending test at CMOD = 0.18 mm analysed with the nonlocal approach. Light grey corresponds to values of $\varepsilon_1 < 0$ whereas black colour corresponds to values of $\varepsilon_1 > 10^{-3}$.

Fig. 8. Contour plots of the maximum principal strain ε_1 of the three point bending test at CMOD = 0.18 mm analysed with the crack band approach. Light grey corresponds to values of $\varepsilon_1 < 0$ whereas black colour corresponds to values of $\varepsilon_1 > 10^{-3}$.

failure in absence of shear reinforcement. The geometry, loading setup and experimental fracture patterns, and the meshes used in the analysis are shown in Figs. 9 and 10, respectively. Due to symmetry, only half of the specimen was analysed by constraining the horizontal displacements of the nodes lying on the symmetry plane. Direct displacement control was applied using the vertical displacement at the bottom of the midspan of the beam. The stress state in the beam during the failure process is triaxial, neither satisfying plane stress nor plane strain conditions [3]. However, in order to reduce the computational time, so that mesh dependence could be studied, the concrete was modelled by 2D plain strain triangular elements.

The procedure to calibrate the two material models and the list of the input parameters are presented in Section 3. The initial analyses are performed with a nonlocal radius of $R = 0.01$, which is considerably larger than the one determined experimentally for a different type of concrete in [31]. However, smaller values of R would require smaller mesh sizes to ensure that there are enough material points within the interaction domain for the calculation of the nonlocal averages, which would increase the computational time for the present implementation of the constitutive law so much that the mesh dependence study performed here would not be possible. It is emphasised that the computational time required could be reduced by parallel computations. Symmetry was taken into account in the material models by modifying the material properties of the points lying close to the symmetry line. In the crack-band approach the fracture energy was assumed to be half of the calibrated value, as proposed by Jirásek and Bauer [18], whereas in the nonlocal approach symmetric local state variable fields were assumed on the other side of the symmetry line. Steel plates were modelled to be linear elastic with Young's modulus $E = 200$ GPa and Poisson's ratio $\nu = 0.3$. The same constitutive law was applied to describe the response of the longitudinal reinforcement, which was modelled explicitly by truss elements. Perfect bond was assumed between steel and concrete for both the nonlocal and crack band analyses in order to simplify the computational problem. This is an idealisation of the interaction of reinforcement and concrete, which might influence the predicted crack patterns and load-displacement curves. However, the present paper focuses mainly on the mesh dependence of the nonlocal concrete material model. Furthermore, in Jendele and Cervenka [17], it was shown that the adoption of an elaborate bond model might lead to numerical stability issues and does not influence the results significantly, if a fine enough mesh has been used, which is the case in the present simulations. Nevertheless, the influence of bond-slip on the fracture should be investigated in future studies.

Coarse, medium and fine meshes with element sizes $h = 0.02$, 0.01 and 0.005 m, respectively, were used to study any possible mesh dependence. The corresponding load–displacement curves are shown in Fig. 11. Furthermore, the evolution of the failure process is illustrated in Figs. 12 and 13 using contour plots of the maximum tensile principal strain ε_1 for the medium mesh for loading steps marked in Fig. 11, as well as contour plots of tensile damage and first principal plastic strain. In addition, the influence of the mesh size on the crack patterns is shown in Fig. 14. The overall failure process observed in the experiments is well reproduced by both models. At early loading stages, vertical failure zones appear in the region of high moment that correspond to the experimentally observed bending cracks (Fig. 12). At about 75% of the peak load, diagonal failure zones develop close to the reinforcement and propagate towards the support and the load application point, which is in accordance with the shear band observed in the original experiments. The failure patterns observed in the model is

Please cite this article as: D. Xenos, P. Grassl, Modelling the failure of reinforced concrete with nonlocal and crack band approaches using the damage-plasticity model CDPM2, Finite Elem. Anal. Des. (2016), http://dx.doi.org/10.1016/j.finel.2016.04.002

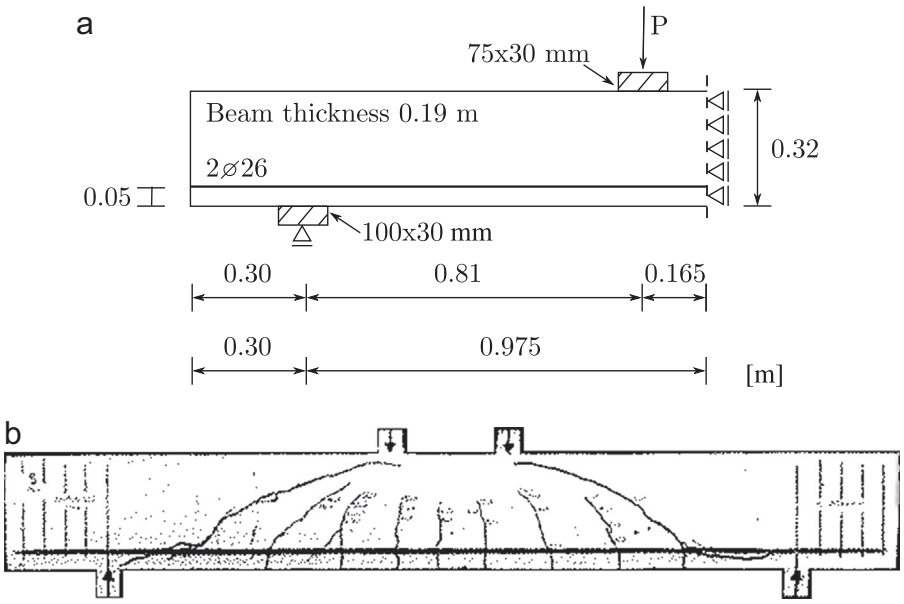

Fig. 9. (a) Geometry and setup, and (b) experimental crack patterns of the reinforced concrete beam [21].

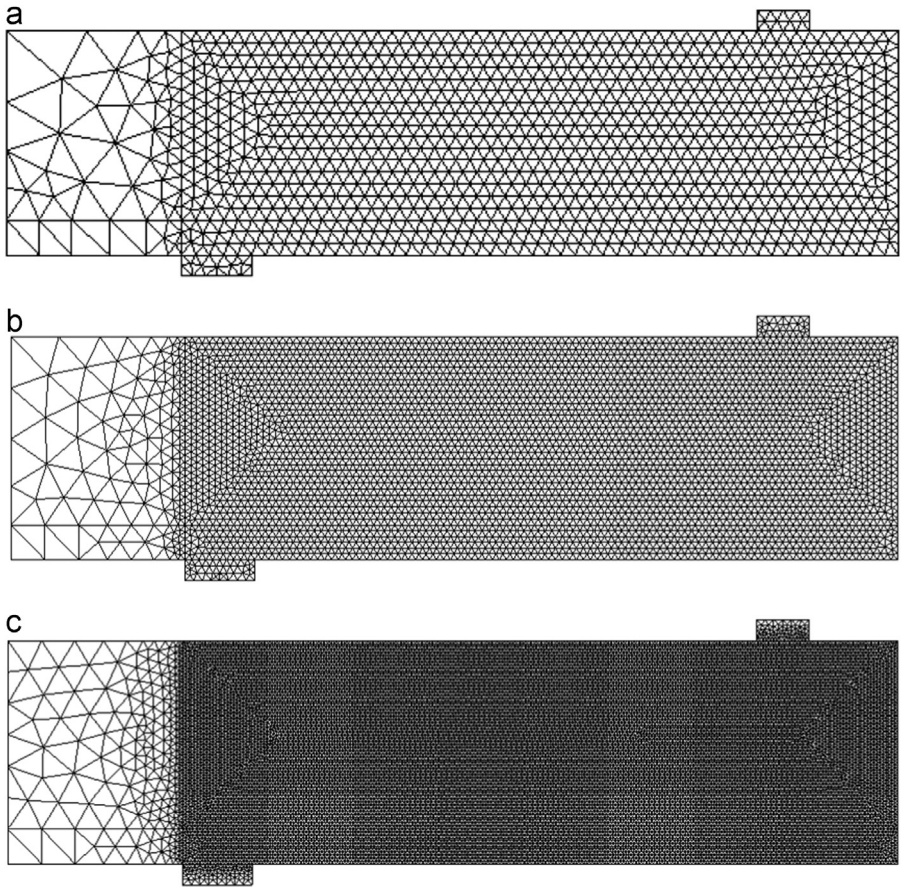

Fig. 10. Analysed mesh sizes: (a) coarse mesh, (b) medium mesh, and (c) fine mesh.

also in agreement with the experimental ones (Fig. 9) and observations reported for similar experimental campaigns [3,30]. However, the inclination of the main crack in the simulations (ca. 45°) is steeper than in the experiments in Fig. 9 (ca. 30°). This difference might be due to the modelling the beam in plane strain and assuming perfect bond between reinforcement and concrete. The load–displacement curves in Fig. 11 are in reasonable agreement with the experimental results. The initial stiffness is overestimated by both approaches. Again, this could be attributed to the use of the plane strain assumption. However, it is more likely that Young's modulus determined using the CEB-FIP Model Code 2010 overestimates the one in the experiments. In both approaches, the

Please cite this article as: D. Xenos, P. Grassl, Modelling the failure of reinforced concrete with nonlocal and crack band approaches using the damage-plasticity model CDPM2, Finite Elem. Anal. Des. (2016), http://dx.doi.org/10.1016/j.finel.2016.04.002

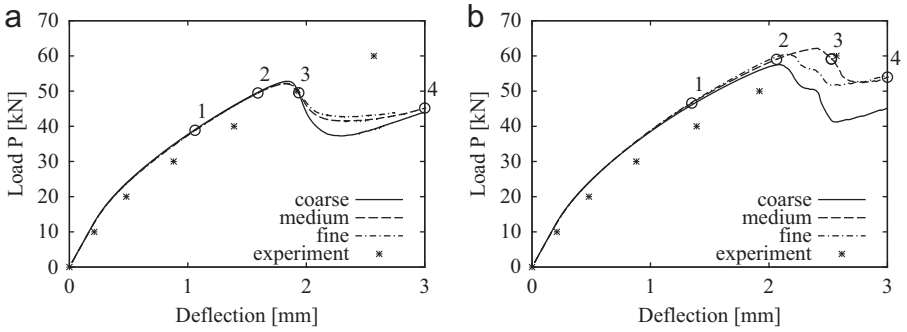

Fig. 11. Load–deflection curve for the reinforced concrete beam [21] analysed for three different meshes with the (a) nonlocal and (b) crack band approach. Deflection is measured at the lowest point at the midspan of the beam.

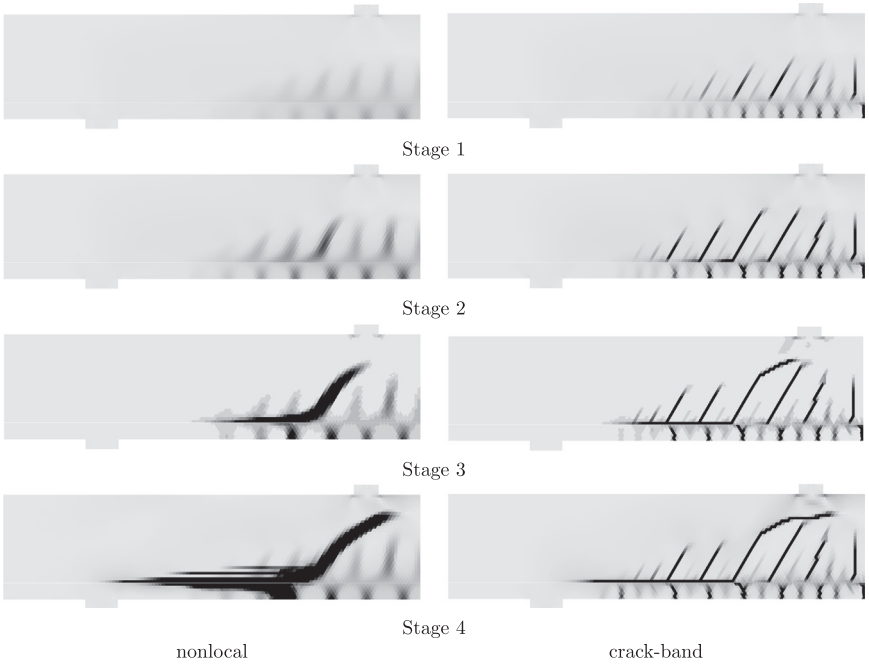

Fig. 12. Evolution of the contour plot of the maximum tensile principal strain ε_1 of the shear beam [21] for the medium mesh at the three loading stages marked in Fig. 11. Light grey colour corresponds to values of $\varepsilon_1 < 0$ whereas black colour corresponds to values of $\varepsilon_1 > 10^{-3}$.

tensile damage and the plasticity part are important to describe this failure mode. Moreover, both constitutive models are not influenced by the mesh size for low load levels. However, nearer to the peak, the two approaches perform differently. For the nonlocal approach, an almost mesh independent response up to the peak is observed (Fig. 11(a)). The response for the coarse mesh differs very slightly, which is explained by studying the strain contour plots for this mesh in Fig. 14. This shows that the mesh is so coarse that only very few integration points are located within the zone considered for the nonlocal averaging. Therefore, a less accurate description of the constitutive response is obtained. Nevertheless, the difference between the results for the three meshes is still very small. On the other hand, the use of the crack-band approach results in mesh dependent peak loads and post-peak responses. There is no clear trend visible in respect of mesh size, as the lowest and highest load capacities are obtained with the coarse and medium mesh, respectively, bracketing the peak of the fine mesh. The mesh dependence for the crack-band approach is also illustrated in Fig. 14, where the contours of ε_1 at the loading stage 3, marked in Fig. 11(b), are shown. The smaller the mesh size is, the larger is the number and the width of the final failure zones and the smaller is their width. This difference in the final crack patterns is the main reason why the load–displacement curves are not converging for decreasing mesh size. The mesh arrangement does not influence the orientation of the final failure zones.

All nonlocal analyses underestimate the peak load, which may be attributed to the selected interaction radius R. However, no attempt was made to adjust the input parameters to obtain a better fit, as the focus was to investigate the influence of mesh size on the model response. Nevertheless, it is illustrative to investigate the influence of R to highlight the fundamental differences in representing the failure zones in crack band and nonlocal approaches. Therefore, an additional analysis for the fine mesh with a smaller radius of $R=0.005$ m was performed. All model parameters except for ε_{ft} were the same as the ones applied for $R=0.01$ m. The damage parameter ε_{ft} was determined from the calibration procedure shown in Section 3 and was equal to 0.00179. The effect of R on the load–displacement curves is shown in Fig. 15. Furthermore, the contour plot of ε_1 is presented in Fig. 16 for loading stage 3 marked in Fig. 15. The interaction radius R has a strong influence on the results. With $R=0.005$ m a higher load capacity was obtained, and more and narrower failure zones were observed in the analyses than for $R=0.01$ m. As it happens, the predicted peak load for this parameter set is in better agreement with the experimental one (Fig. 15) than for $R=0.01$ m. For the same increase of the beam deflection, a larger decrease of the

Please cite this article as: D. Xenos, P. Grassl, Modelling the failure of reinforced concrete with nonlocal and crack band approaches using the damage-plasticity model CDPM2, Finite Elem. Anal. Des. (2016), http://dx.doi.org/10.1016/j.finel.2016.04.002

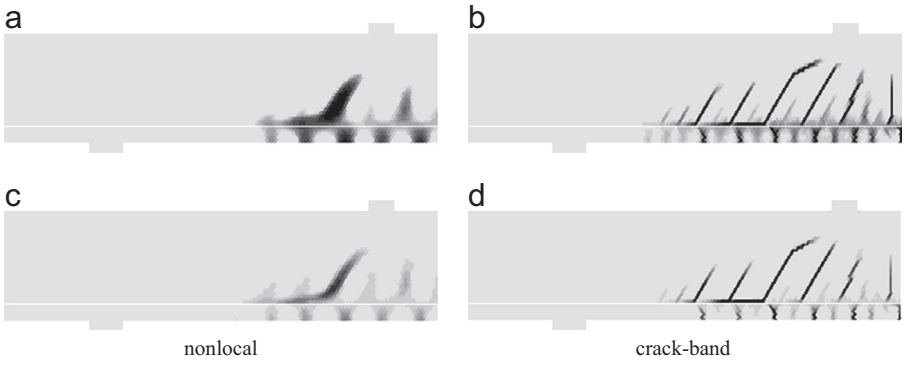

Fig. 13. Contour plots of the (a), (b) tensile damage variable ω_t and (c), (d) the first principal plastic strain ε_{p1} for the medium mesh at loading stage 3 marked in Fig. 11. Light grey colour corresponds to values of ω_t and ε_{p1} equal to 0 whereas black colour corresponds to values of $\omega_t = 1$ and $\varepsilon_{p1} > 0.005$.

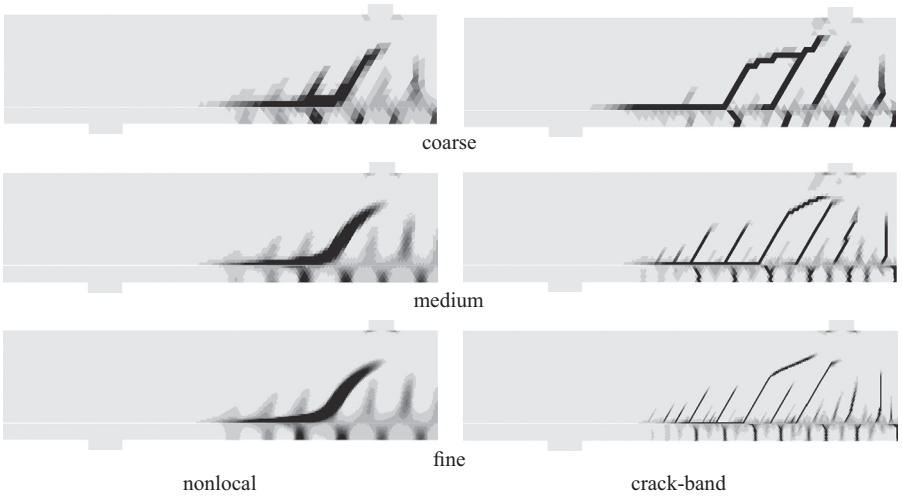

Fig. 14. Contour plots of the maximum tensile principal strain ε_1 of the shear beam [21] for all mesh sizes at loading stage 3, marked in Fig. 11. Light grey colour corresponds to values of $\varepsilon_1 < 0$ whereas black colour corresponds to values of $\varepsilon_1 > 10^{-3}$.

applied load is observed for $R=0.01$ m than for $R=0.005$ m, which is not in accordance with similar studies performed for experimental setups where a single localisation zone is observed [7]. However, multiple failure zones form in this experiment and therefore the arrangement of the failure zones predicted for a certain value of R results in different loading histories of the material points and in different global load–displacement curves. It is also noted that no attempt was made to fit R to match the load–displacement curve. The interaction radius R in the nonlocal approach has a similar influence as the mesh size in the crack-band approach. The main difference between the two approaches is that R is a material parameter, which is independent of the mesh size. Consequently, in nonlocal models crack spacing is, among others, influenced by the choice of the material parameter R, whereas in crack band approaches it depends on the numerical discretisation.

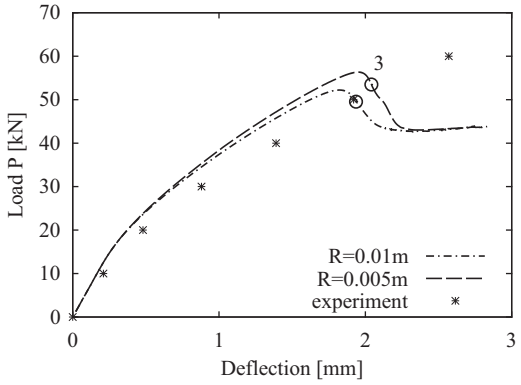

Fig. 15. Load–deflection curve of the reinforced concrete beam [21] analysed for the fine mesh with the nonlocal model with different R. Deflection is measured at the lowest point of the midspan of the beam.

6. Conclusions

The damage-plasticity constitutive law CDPM2, originally presented in Grassl et al. [16], was extended according to the nonlocal and crack-band theory. Both material models were applied to model two plain concrete tests in the form of a one-dimensional bar subjected to direct tension and an unnotched three point bending test. Furthermore, a reinforced concrete beam subjected to four point bending was analysed. For the one-dimensional bar, both models produce mesh independent load–displacement curves. The nonlocal model provides mesh independent strain profiles, whereas for the crack band model, the strain profiles representing the crack depend on the element size. For the beams, the use of the nonlocal model results in mesh independent load–displacement curves and strain crack patterns as long as the mesh size is small enough to ensure that there are enough material points contributing to the nonlocal averaging of the history

Please cite this article as: D. Xenos, P. Grassl, Modelling the failure of reinforced concrete with nonlocal and crack band approaches using the damage-plasticity model CDPM2, Finite Elem. Anal. Des. (2016), http://dx.doi.org/10.1016/j.finel.2016.04.002

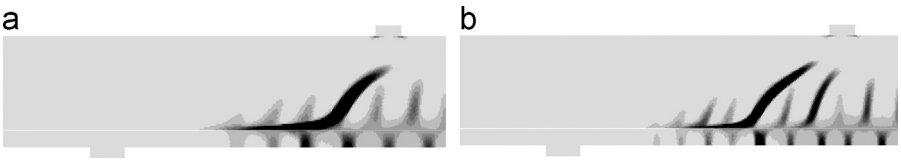

Fig. 16. Contour plots of the maximum tensile principal strain ε_1 of the shear beam [21] at loading stage 3, marked in Fig. 15, for the fine mesh analysed with the nonlocal approach for (a) $R=0.01$ m and (b) $R=0.005$ m. Light grey colour corresponds to values of $\varepsilon_1 < 0$ whereas black colour corresponds to values of $\varepsilon_1 > 10^{-3}$.

variables. For the crack band approach, both the load–displacement curves and the crack patterns are mesh dependent.

Acknowledgements

P. Grassl acknowledges funding received from the UK Engineering and Physical Sciences Research Council (EPSRC) under Grant EP/I036427/1 and funding from Radioactive Waste Management Limited (RWM) (http://www.nda.gov.uk/rwm), a wholly-owned subsidiary of the Nuclear Decommissioning Authority. RWM is committed to the open publication of such work in peer reviewed literature, and welcomes e-feedback to http://www.rwmdfeedback@nda.gov.uk. The numerical analyses have been performed with OOFEM, an open-source object-oriented finite element program [27] extended by the present authors. The finite element meshes have been prepared with the T3D mesh generator [29].

References

[1] Z.P. Bažant, Nonlocal damage theory based on micromechanics of crack interactions. J. Eng. Mech., ASCE 120 (1994) 593–617.
[2] Z.P. Bažant, M. Jirásek, Nonlocal integral formulations of plasticity and damage: survey of progress. J. Eng. Mech., ASCE 128 (2002) 1119–1149.
[3] Z.P. Bažant, M.T. Kazemi, Size effect on diagonal shear failure of beams without stirrups, ACI Struct. J. 88 (1991) 268–276.
[4] Z.P. Bažant, J.L. Le, C.G. Hoover, Nonlocal boundary layer (NBL) model: Overcoming boundary condition problems in strength statistics and fracture analysis of quasibrittle materials, in: Fracture Mechanics of Concrete and Concrete Structures, JeJu, Korea, 2010, pp. 135–143.
[5] Z.P. Bažant, B.H. Oh, Crack band theory for fracture of concrete, Mater. Struct. 16 (1983) 155–177.
[6] Z.P. Bažant, G. Pijaudier-Cabot, Measurement of characteristic length of nonlocal continuum, J. Eng. Mech., ASCE 115 (1989) 755–767.
[7] C.L. Bellégo, J.F. Dubé, G. Pijaudier-Cabot, B. Gérard, Calibration of nonlocal damage model from size effect tests, Eur. J. Mech. A/Solids 22 (2003) 33–46.
[8] J. Bolander, H. Hikosaka, Simulation of fracture in cement-based composites, Cement Concr. Compos. 17 (1995) 135–145.
[9] FIB, FIB-Model Code for Concrete Structures 2010, International Federation for Structural Concrete (FIB), 2012.
[10] S. Fichant, C.L. Borderie, G. Pijaudier-Cabot, Isotropic and anisotropic descriptions of damage in concrete structures, Mech. Cohes. Frict. Mater. 4 (1999) 339–359.
[11] C. Giry, F. Dufour, J. Mazars, Stress-based nonlocal damage model, Int. J. Solids Struct. 48 (2011) 3431–3443.
[12] P. Grassl, Modelling of dilation of concrete and its effect in triaxial compression, Finite Elem. Anal. Des. 40 (2004) 1021–1033.
[13] P. Grassl, M. Jirásek, Damage-plastic model for concrete failure, Int. J. Solids Struct. 43 (2006) 7166–7196.
[14] P. Grassl, M. Jirásek, A plastic model with nonlocal damage applied to concrete, Int. J. Numer. Anal. Methods Geomech. 30 (2006) 71–90.
[15] P. Grassl, D. Xenos, M. Jirásek, M. Horák, Evaluation of nonlocal approaches for modelling fracture near nonconvex boundaries, Int. J. Solids Struct. 51 (2014) 3239–3251.
[16] P. Grassl, D. Xenos, U. Nyström, R. Rempling, K. Gylltoft, CDPM2: a damage-plasticity approach to modelling the failure of concrete, Int. J. Solids Struct. 50 (2013) 3805–3816.
[17] L. Jendele, J. Cervenka, Finite element modelling of reinforcement with bond, Comput. Struct. 84 (2006) 1780–1791.
[18] M. Jirásek, M. Bauer, Numerical aspects of the crack band approach, Comput. Struct. 110–111 (2012) 60–78.
[19] M. Jirásek, P. Grassl, Evaluation of directional mesh bias in concrete fracture simulations using continuum damage models, Eng. Fract. Mech. 75 (2008) 1921–1943.
[20] A. Krayani, G. Pijaudier-Cabot, F. Dufour, Boundary effect on weight function in nonlocal damage model, Eng. Fract. Mech. 76 (2009) 2217–2231.
[21] F. Leonhardt, R. Walther, Schubversuche an einfeldrigen Stahlbetonbalken mit und ohne Schubbewehrung zur Ermittlung der Schubtragfähigkeit und der oberen Schubspannungsgrenze, DAfStb-Deutscher Ausschuss für Stahlbeton, 1962.
[22] T. Majewski, J. Bobinski, J. Tejchman, FE analysis of failure behaviour of reinforced concrete columns under eccentric compression, Eng. Struct. 30 (2008) 300–317.
[23] J. Mazars, Application de la mécanique de l'endommagement au comportement non linéaire et à la rupture du béton de structure (Thèse de Doctorat d'Etat), Université Paris VI, France, 1984.
[24] P. Menétrey, K.J. Willam, A triaxial failure criterion for concrete and its generalization, ACI Struct. J. 92 (1995) 311–318.
[25] M. Ortiz, A constitutive theory for the inelastic behavior of concrete, Mech. Mater. 4 (1985) 67–93.
[26] J. Pamin, R. De Borst, Simulation of crack spacing using a reinforced concrete model with an internal length parameter, Arch. Appl. Mech. 68 (1998) 613–625.
[27] B. Patzák, OOFEM—an object-oriented simulation tool for advanced modeling of materials and structures, Acta Polytech. 52 (2012) 59–66.
[28] G. Pijaudier-Cabot, Z.P. Bažant, Nonlocal damage theory, J. Eng. Mech., ASCE 113 (1987) 1512–1533.
[29] D. Rypl, Sequential and parallel generation of unstructured 3D meshes (Ph.D. thesis), Czech Technical University. Prague, Czech Republic, 1998.
[30] F. Vecchio, W. Shim, Experimental and analytical reexamination of classic concrete beam tests, J. Struct. Eng. 130 (2004) 460–469.
[31] D. Xenos, D. Grégoire, S. Morel, P. Grassl, Calibration of nonlocal models for tensile fracture in quasi-brittle heterogeneous materials, J. Mech. Phys. Solids 82 (2015) 48–60.

Please cite this article as: D. Xenos, P. Grassl, Modelling the failure of reinforced concrete with nonlocal and crack band approaches using the damage-plasticity model CDPM2, Finite Elem. Anal. Des. (2016), http://dx.doi.org/10.1016/j.finel.2016.04.002